Journal of Nuclear Materials xxx (2013) xxx–xxx

Contents lists available at SciVerse ScienceDirect

Journal of Nuclear Materials

journal homepage: www.elsevier.com/locate/jnucmat

Measurement and modeling of surface temperature dynamics of the NSTX liquid lithium divertor

A.G. McLean [a,*,1], K.F. Gan [b], J.-W. Ahn [c], T.K. Gray [c], R. Maingi [c], T. Abrams [d], M.A. Jaworski [d], R. Kaita [d], H.W. Kugel [d], R.E. Nygren [e], C.H. Skinner [d], V.A. Soukhanovskii [a]

[a] Lawrence Livermore National Laboratory, Livermore, CA 94551, USA
[b] Institute of Plasma Physics, Chinese Academy of Sciences, Hefei, People's Republic of China
[c] Oak Ridge National Laboratory, Oak Ridge, TN 37831, USA
[d] Princeton Plasma Physics Laboratory, Princeton, NJ 08543, USA
[e] Sandia National Laboratories, Albuquerque, NM 87185, USA

ARTICLE INFO

Article history:
Available online xxxx

ABSTRACT

Dual-band infrared (IR) measurements of the National Spherical Torus eXperiment (NSTX) Liquid Lithium Divertor (LLD) are reported that demonstrate liquid Li is more effective at removing plasma heat flux than Li-conditioned graphite. Extended dwell of the outer strike point (OSP) on the LLD caused an incrementally larger area to be heated above the Li melting point through the discharge leading to enhanced D retention and plasma confinement. Measurement of $T_{surface}$ near the OSP demonstrates a significant reduction of the LLD surface temperature compared to that of Li-coated graphite at the same major radius. Modeling of these data with a 2-D simulation of the LLD structure in the DFLUX code suggests that the structure of the LLD was successful at handling up to $q_{\perp,peak}$ = 5 MW/m^2 inter-ELM and up to 10 MW/m^2 during ELMs from its plasma-facing surface as intended, and provide an innovative method for inferring the Li layer thickness.

1. Introduction

Since 2008, the benefits associated with the use of evaporated Lithium (Li) for surface conditioning in NSTX have been well documented, notably for pedestal performance and ELM suppression [1,2]. More recently, Li has been found to be compatible with advanced divertor configurations [3] and long-pulse operation [4] confirming the potential for a role for lithiated plasma-facing surfaces in next-step devices. To extend investigation of a pure lithiated surface in a tokamak to density and impurity control, the liquid lithium divertor (LLD) was installed in NSTX in 2010 [5,6]. Precise knowledge of the thermal dynamics for the Li plasma-facing surface and the heat flux the LLD is exposed to is required both for physical interpretation of the influence of Li on plasma performance and tokamak operation, and to ensure engineering limits for the LLD structure are not exceeded. This is especially important for a spherical tokamak (ST) like NSTX which can exceed 15 MW/m^2 during transient events [7] and the presence of localized hot spots and impurity sources must be minimized.

Use of Lithium (Li) beyond that of a conditioning material, however, presents challenges for characterization of the Li plasma facing surface with available boundary diagnostics and control of its response to high heat flux [8]. In particular, the vastly different emissivity of molten Li ($\varepsilon < 0.1$) compared to that of graphite ($\varepsilon > 0.85$), and its variability with temperature and composition makes interpretation of infrared (IR) emission difficult for measurement of absolute surface temperature and thus determination of impinging heat flux. Similar challenges exist for accurate interpretation of visible spectroscopy, and accounting for losses in optical transmission by vacuum components on which highly mobile Li can a deposit. In this paper, the LLD thermal response to direct plasma contact as monitored using an innovative dual-band IR camera are presented and the implications for associated plasma response are discussed.

2. Apparatus and experiments

Installed in NSTX for operation in the 2010 plasma campaign, the LLD is composed of four heated plates extending radially from R = 0.66 to 0.85 m and toroidally around the outboard divertor separated by gaps for diagnostic graphite tiles (Fig. 1). LLD plates are made primarily of copper covered by a thin layer of stainless steel and a top layer of porous Molybdenum (Mo) into which Li is evaporated between discharges at two toroidal locations from top of the

* Corresponding author. Address: General Atomics, 3483 Dunhill Street, MS 13-355, San Diego, CA 92121-1215, USA.
E-mail address: mclean@fusion.gat.com (A.G. McLean).
[1] Presenting author.

0022-3115/$ - see front matter © 2013 Published by Elsevier B.V.
http://dx.doi.org/10.1016/j.jnucmat.2013.01.079

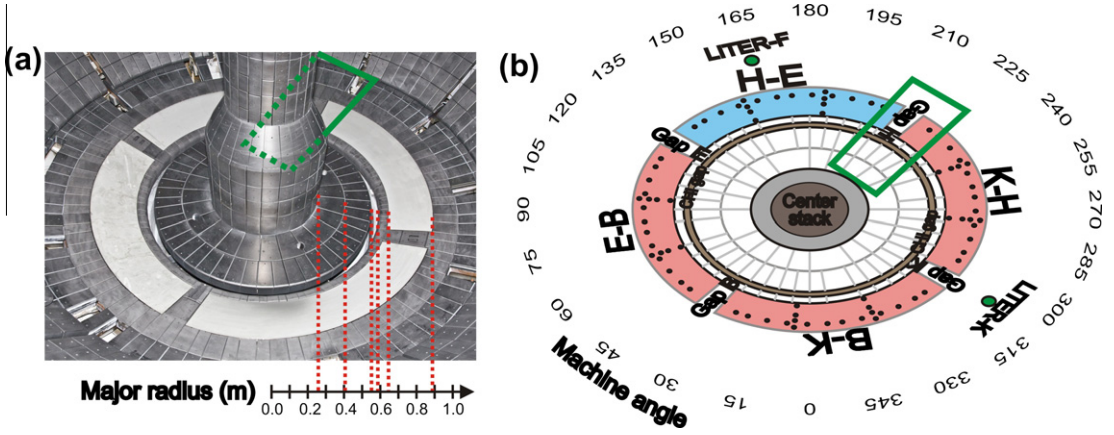

Fig. 1. (a) View in the NSTX vessel prior to the 2010 campaign showing the location of all four LLD plates and the radial location of major divertor features. (b) Schematic representation of the LLD plates labeled by their alphabetic designations, the toroidal locations of the two Li evaporator locations, and the embedded thermocouples used for IR camera calibration. The R, φ viewing extent of the dual-band IR camera is shown in green. (For interpretation of the references to colour in this figure legend, the reader is referred to the web version of this article.)

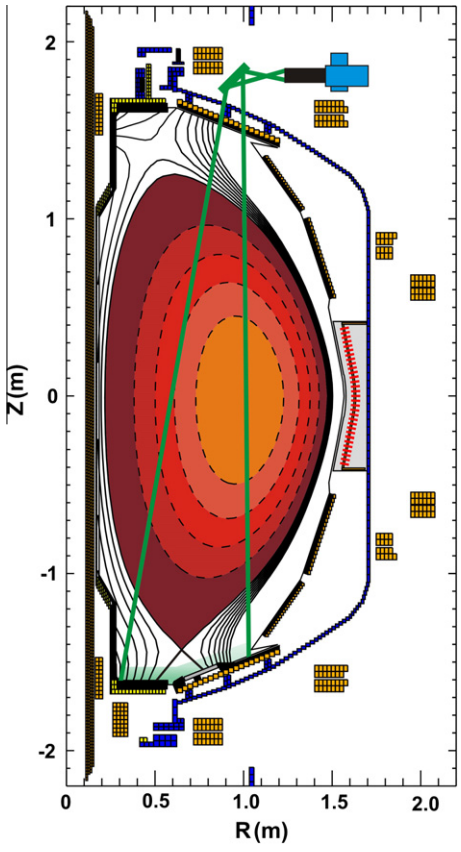

Fig. 2. NSTX poloidal cross-section showing the viewing geometry of the dual-band fast IR camera from the top of the machine $(R,Z) = \sim(1.5, 1.8\ \text{m})$, and a magnetic equilibrium typical for exposure of the LLD to the OSP.

machine [6,9]. Throughout the campaign, the LLD surface was heated up to and beyond the melting point of Lithium, $T_{melt,Li} = 180.54\ ^\circ\text{C}$, both prior to a plasma discharge by electrical or hot air heating of its copper substrate, and by exposure to successive plasma discharges.

High-speed, 2-D temperature dynamics of the NSTX lower divertor surface ($\sim 0.27\ \text{m} < R < \sim 0.85\ \text{m}$, $\sim 210^\circ < \varphi < \sim 228^\circ$) were measured by a fast IR imaging system [10] at the top of the machine (Fig. 2) retrofitted with dual-band capability in order to overcome the complexity introduced by changes in scene emissivity and aid in compensating for transmission losses due to Li accumulation on the vacuum window [11]. The camera was absolutely calibrated *ex situ* using blackbody sources, and *in situ* during vessel bake procedures and during heating of the LLD plates where embedded thermocouples provide temperature data for each plate individually. During post-discharge cooling of the LLD surface, the latent heat of fusion is properly indicated by thermal decay to the Li freezing temperature on the LLD surface, compared with a simultaneous and continuous decay in surface temperature of Li-coated graphite temperature below the Li melting point without a plateau at $T_{melt,Li}$.

Lower single null (LSN) discharges were operated with the outer strike point (OSP) on the LLD plates (Fig. 2) with up to $P_{NBI} = 4$ MW, $I_p = 1.2$ MA, $B_T = 0.5$ T, and $T_{surface,LLD} = 320\ ^\circ\text{C}$ prior to plasma exposure. The LLD bulk temperature was found to rise by $\sim$5–10 °C per discharge with plasma heating alone. During the highest energy discharges, the LLD survived direct, peak perpendicular heat flux of up to $q_{\perp,peak} = 5\ \text{MW/m}^2$ inter-ELM and up to $10\ \text{MW/m}^2$ during ELMs through 12 operational days without significant damage to the porous Mo surface. Of particular interest for the present work are two series' of 10 similar and sequential plasma discharges with a steady OSP in contact with the LLD for $\sim$0.5 s per discharge lasting 0.8–1.0 s starting at 0.3 s. Thermal response of the LLD during these discharges and trends in plasma parameters through each series are particularly revealing in understanding the role of Li as a plasma-facing material.

3. Results and discussion

Two features of the LLD thermal response to plasma contact are of particular interest for interpretation of transient features in plasma performance measured in NSTX and associated with the LLD [1,6], and the effectiveness of Li as a first-wall material. First, the temporal response of the LLD to plasma exposure is revealed and examined by repeated exposure to the OSP over the course of 10 moderate power discharges (Fig. 3). Through the OSP dwell in the first discharge, the area in which the temporarily averaged surface temperature is measured to be $> T_{melt,Li}$ is $\sim$30% (Fig. 3a). This region extends $\sim$4–5 cm outboard and $\sim$1–2 cm inboard of the OSP location. By the 10th discharge in the series, however, the fractional area with $T_{avg} > T_{melt,Li}$ is $\sim$90% (Fig. 3b). Additionally, the peak average surface temperature has increased through the series

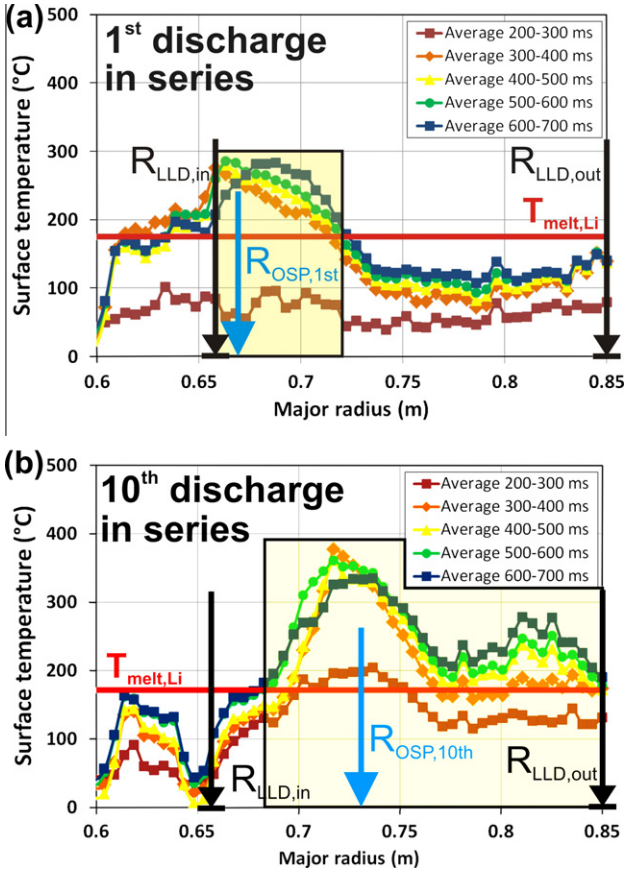

Fig. 3. IR-measured surface temperature versus major radius averaged through 100 ms periods at (a) the beginning of a series of sequential discharges exposing the LLD to the OSP, and (b) at the end. The fractional area of the LLD at $>T_{melt,Li}$ in the first discharge (highlighted between the radial edges of the LLD surface, $0.66 < R < 0.85$ m) is ~30% in the first discharge, increasing to ~90% by the 10th discharge in the series.

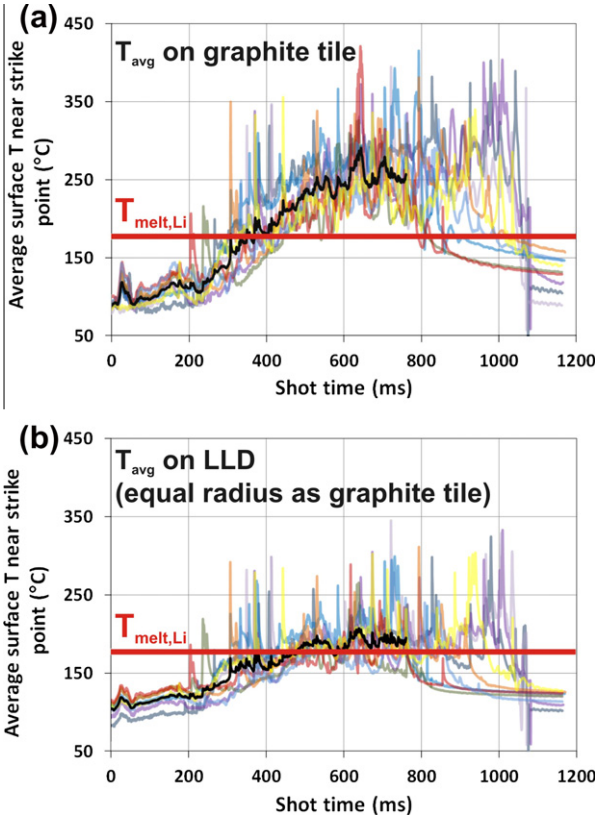

Fig. 4. Average surface temperature measured within ±2 cm of the OSP is shown in 10 sequential repeat discharges plotted versus shot time. In (a), the temperature is that of the Gap H graphite tile, and in (b) is the temperature measured simultaneously at the same radial location but toroidally displaced to the LLD surface. The near-OSP temperature averaged over all 10 discharges is ~60–70 °C lower on the LLD compared to the graphite tile.

by <100 °C (from ~280 °C in the first discharge to ~350 °C in the tenth), which is ~equal to the increase in the LLD surface temperature measured prior to the OSP dwell (from ~50 °C measured just prior to plasma contact in the first discharge to ~100 °C in the tenth). Also, the areal melted fraction of the LLD surface once constant plasma contact is applied does not change significantly within any single discharge. Neither does the temporally-averaged peak temperature increase in a continuous manner; instead, the radial thermal distribution reached by ~300 ms into the discharge remains relatively steady until termination of the discharge. These observations suggest that the primary direction of heat transfer on timescales of ~0.1 s is into the bulk of the LLD, not radial, supporting the role of the LLD as an effective plasma-surface structure in the presence of high heat flux. It is also of note that the presence of a second bump in the radial temperature profile well outboard of the OSP present in data from the 10th discharge (centered at $R \sim 0.82$ m) suggests that significant heating has occurred as a consequence of non-axisymmetric lobes present due to error fields in the machine [12,13].

A second observation revealing the effectiveness of the LLD as a plasma-facing surface is shown in the comparison of the radially average temperature near the OSP on the Li surface versus that of a nearby graphite tile (see Fig. 1). In a second series of 10 repeat discharges, the LLD is heated to 70 °C prior to each plasma exposure and allowed to cool back to this temperature afterwards. The average temperature within ±2 cm of the OSP location both on the LLD, and at the same radial location but toroidally displaced on the nearby graphite gap tile is plotted versus time for all 10 discharges (Fig. 4). The average for all 10 discharges is also plotted for each location versus time for the period extending to the termination of the shortest discharge in a single heavy line. By the end of this time, the trend in the 10-discharge average is ~60–70 °C cooler on the LLD versus on a graphite tile. This observation supports the premise that the LLD was effective at heat removal when exposed to the OSP as intended in the design. Additionally, a short delay (~100 ms) is seen in the LLD-averaged data at $T_{melt,Li}$ prior to increasing above 180 °C which is not apparent in the data viewing the tiles, consistent with the enthalpy of fusion playing a role in the temperature trend. Finally, the thermal excursions measured on both the graphite and the LLD surface due to ELMing events are found to be of similar magnitude, suggesting that thermal parameters of the surface layer on each surface have similar effective thermal properties.

Finally, the thermal response of the structure of the LLD has been modeled in a new 2-D numerical heat conduction code, DFLUX [14]. The code employs a realistic cross-sectional geometry and temperature-dependent material thermal parameters to effectively model transient behavior, especially phase changes in Li. Also included is an enhanced heat transmission factor, α, to account for loosely-adhered deposit layers present on the plasma-facing surface equivalent to that incorporated in the THEODOR code. Modeling of the experimental thermal data from the discharges discussed confirms that suppression of heating on the LLD compared to lithiated graphite, likely due to (a) higher heat capacity of Li in the LLD versus ATJ graphite where deposited Li is subject to erosion and transport, and (b) greater thermal

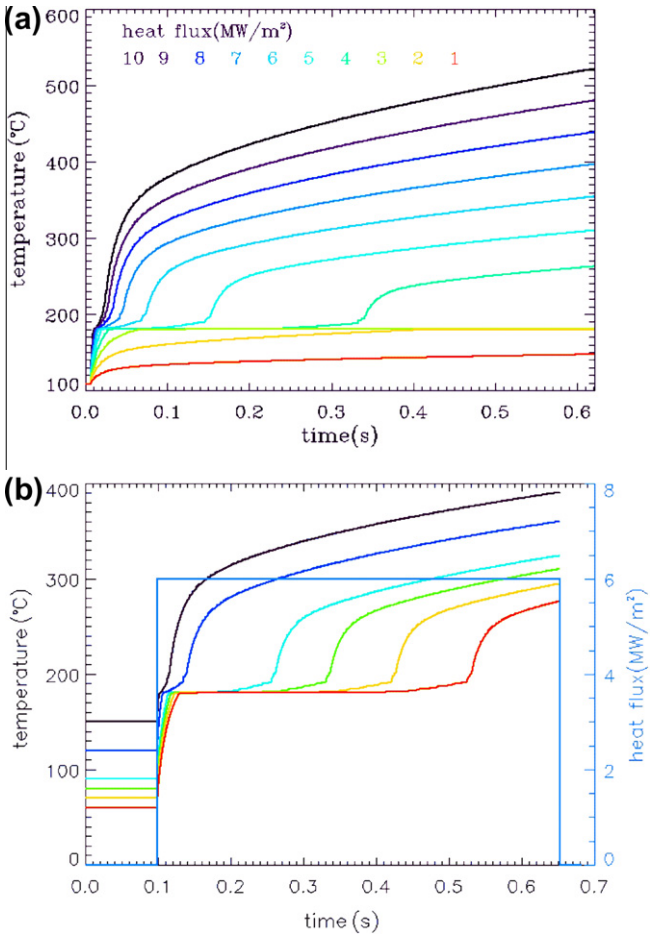

Fig. 5. Results from DFLUX modeling showing the impact on the duration for heat, or enthalpy, of fusion (i.e., melting) of (a) varying the impinging heat flux to the LLD surface, and (b) varying the initial layer temperature from 50 to 150 °C but under constant heat flux of 5 MW/m^2. Both results may also be applied to the opposing case where heat flux to the surface is removed and Li cools to the point of freezing.

conductivity of Li at $T > 300$ °C. The code also strongly suggests Li deposited on graphite tiles forms loosely adheared layers; here $\alpha \sim 60$ kW/m^2/K is suggested. Additional tests with the code demonstrate that the time for phase change of Li to occur (the enthalpy of fusion) both during heating and cooling of the LLD are highly dependent on each of (a) the Li layer thickness, (b) the magnitude of the impinging heat flux the initial layer temperature prior to plasma heating (Fig. 5a) and (c), the initial layer temperature prior to plasma heating (Fig. 5b). Based on these observations, comprehensive modeling of a discharge in the first series discussed here suggests the Li layer thickness on the LLD is 0.2–0.4 mm. Additional modeling of these discharges with DFLUX will be the subject of a future publication.

It should be pointed out that collectively these results, and those demonstrating the enthalpy of fusion of Li presented in [11] validating the application of the dual-band technique, suggest only that the dominant material driving the thermal response is pure Li. The existence of a very thin (nm scale) top layer consisting of lithiated compounds due to uptake of C, O, and other impurities as suggested in [15,16] cannot be ruled out. Further investigation into thermal signature of such layers in the experimental data and by way of modeling are planned.

4. Conclusions

The dynamic thermal response of the LLD plasma-facing surface in NSTX has been measured by a fast, dual-band IR diagnostic, revealing important ways the liquid lithium surface reacts to high heat flux with extended plasma exposure. Extended dwell of the strike point on the LLD caused an incrementally larger area to be heated above the Li melting point through the discharge suggesting a possible mechanism for observed enhanced D retention and improved plasma confinement [7,16]. Measurement of $T_{surface}$ near the OSP demonstrates a significant suppression of the LLD surface temperature compared to that of Li-coated graphite at the same major radius, supporting the power handling performance of the LLD. Modeling of these data with a 2-D simulation of the LLD structure in the DFLUX code confirms these observations and suggests an innovative method for inferring the Li layer thickness. Additional comprehensive modeling of the LLD response is planned with DFLUX in the future.

Acknowledgement

This work was supported by the US Department of Energy, Contract numbers DE-AC05-000R22725, DE-AC52-07NA27344, and DE-AC02-09CH11466.

References

[1] M.G. Bell et al., Plasma Phys. Control. Fusion 51 (2009) 124054.
[2] R. Maingi et al., Phys. Rev. Lett. 103 (2009) 075001.
[3] V. Soukhanovskii, et al., This conference.
[4] X. Gong, et al., This conference.
[5] H.W. Kugel et al., Phys. Plasmas 15 (2008) 056118.
[6] H.W. Kugel et al., Fusion Eng. Des. 87 (2012) 1724.
[7] T.K. Gray et al., J. Nucl. Mat. 415 (2011) S360.
[8] T. Abrams, et al., This conference.
[9] R. Kaita, et al., This conference.
[10] J.-W. Ahn et al., Rev. Sci. Instrum. 81 (2011) 023501.
[11] A.G. McLean et al., Rev. Sci. Instrum. 83 (2012) 053706.
[12] J-W. Ahn, et al., This conference.
[13] J.D. Lore, et al., This conference.
[14] K.F. Gan, et al., This conference.
[15] F. Scotti, et al., This conference.
[16] C.H. Skinner, et al., This conference.